

## Visualization of Earth Deformation

<sup>1</sup> Sheikh Nasir b. Kamarudin, <sup>2</sup> Dr. Mohd Sharfy bin Mohd Rahim, <sup>3</sup> Nor Anita Fairos bt. Ismail, <sup>4</sup> J.G.Liu, <sup>5</sup> P.Mason  
<sup>1,2,3</sup> ViCube Lab, Faculty of Science & Information System, Johor Bahru  
<sup>3,4</sup> Department of Earth Science and Engineering, Imperial College London, UK  
Email: <sup>1</sup>sheikhnasir@yahoo.com, <sup>2</sup>noranita@utm.my, <sup>3</sup>sharfy@utm.my, <sup>4</sup>liu@th.ic.ac.uk, <sup>5</sup>mason@th.ic.ac.uk

**Abstract.** The rapidly growing field of remote sensing is beginning to supply massive quantities of high-resolution imagery of the Earth and other planets. In the earth sciences, parallel supercomputers have always played a prominent role in the visualization of this imagery, and in other image processing applications designed to enhance and display the obtained information. Imageodesy is a technique for detection and measurement of feature shifts between two images based on local feature fitting algorithms such as Normalize Cross-Correlation (Crippen, 1992) and phase correlation. This technique allows the vast archives of optical imagery, collected by satellite systems such as SPOT and Landsat, to be used not only to detect but also to measure the subtle terrain displacements associated with earthquakes, glacial motion and volcanic processes, all to within sub-resolution accuracy and precision is also a major factor.

**Keywords :** *Imageodesy, Normalize Cross-Correlation, Visualization*

\* Corresponding Author:  
Sheikh Nasir Kamarudin,  
ViCube Lab, Faculty of Science & Information System, Johor Bahru  
Universiti Teknologi Malaysia  
Email: sheikhnasir@yahoo.com Tel:+6016-7075226

### 1. Introduction

Earth Surface crust is moving almost every second. Landslides are down slope movements of rock, debris or earth under the influence of gravity which may cover a wide range of spatial and temporal scales. Most landslides occur at steep slopes, but they can also happen in low relief areas in connection with excavations by rivers or construction work. Landslides can be triggered by natural environmental changes or by human activities. Earthquakes, volcanic activity, heavy rain falls and changes of ground water level are typical natural triggering mechanisms for landslides which amplify the inherent weakness in rock or soil. Landslides may result in severe human casualties, property losses and environmental degradation. Landslide disasters reveal rising costs to society and economy because of significant population increase and development in many of the vulnerable areas.

These small movements (displacement) that occurs are not possible to be seen with our naked eyes since the changes are less than 1 mm. However, these displacements can be seen over durations of times. In order, to obtain this information, satellite technologies are the only solution. Since the satellites are rotating and observing the earth, this information can be very useful to be predicted and planned for future hazard.

Furthermore, with the accumulation of data over the years of time, data mining and data extraction can be used to see the pattern movement based on current technologies. Even though, current available

technique unable to detect the movement with high precision, which the technique called Interferogram. Using InSar, radar technologies which extract phase changes from two InSar images of two different dates. This technique can measured minimum displacement of 100m or bigger shift.

Other than that, there are also higher resolution imageries that have up to less than 1 m resolution. Since these imageries have this feature, better interpretations can be made. Appropriate technique should be used to pin point the location and match the location of both images. When the location can be accurately located, the displacement can be match and marked. Current available Technique that has been proven is Imageodesy, [5] Since the obtained images from these satellites are in pixel based manipulation, these enhanced the previous method from 100 m to less than 1m.

For the purpose of these research and to enhance the detection of this displacement on the land, high resolution satellite such as ASTER with 15 m resolution, IKONOS with less than 1 meter or others will be used.

## 2. Background Study

Prediction has always been an issue to the geologists and has never been very successful due lack of accuracy and also the data to extract the information for observing the trend line of the displacement. However, with the availability raster imagery with high resolution and constant observation, the trend line can be monitored. For instance, Article Distributed, high-performance earthquake deformation analysis and modeling facilitated by Discovery Net [18], has uncover some detection for been investigating the relationship between macro and micro-scale earthquake deformational processes has successfully developed and tested a geoinformatics infrastructure for linking computationally intensive earthquake monitoring and modeling.

On the other hand, these images can have noise or distortion or even other issue which can cause the inaccuracy of the observation. Using Normalized Cross-Correlation these problems can be fixed since it only takes appropriate pixel by pixel match template matching. These has be done and proven effective to match it accurateness. The result obtain from these has a significant details of information that show the displacement shift which resembled to observation made by the Geologist.

Below are the lists of programs used to develop the software and to analyze the information.

- Microsoft Visual C++ 6.0 (MFC)

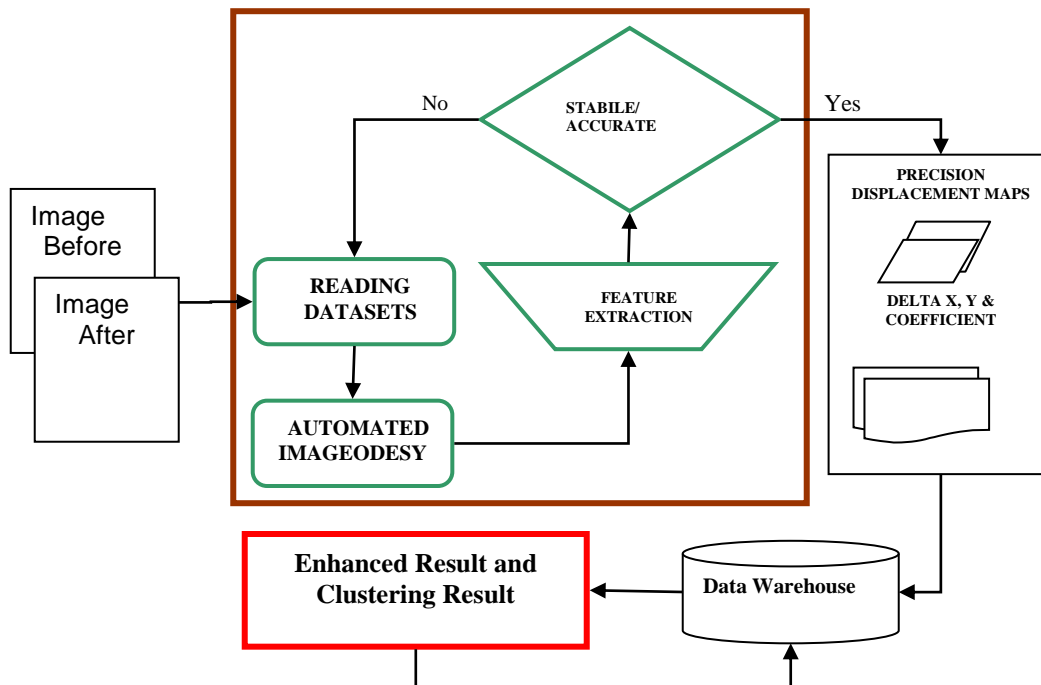


Figure 1: Enhanced Earth Deformation Detection Architecture

- ER Mapper Library (SDK) Version 6.0
- ER Mapper Version 6.2

In order to understand greater details of the techniques used, it is important to understand the structure of the prototype. Next we will describe the architecture of the Prototype, frame works and details of method used.

Figure 1 is the design of the architecture for Earth Deformation detection. The design has 5 modules which will be discussed in the next section. Two images which covered the same areas were loaded to the program. Once the DN array was available, features were extracted after automated imageodesy motion. This module will process and allocate the block DN value for calculation. Each calculation made was kept in an array. If the shift is stable or accurate, which in this case the threshold value has been set in order to select the highest point of correlation. After that, displacement maps and other relevant output were generated for accuracy assessments. If the shift is not stable, inaccurate or out of specific range, it would be ignored based on the Threshold value given on the early setting and a NULL value was registered in the displacement maps, delta X, delta Y and coefficient that match them point in the actual dataset location.

The most important process in the prototype is to keep the coordinate information efficiently and accurately. All of the DN values are keep in the search and target array as declared. The array size could be increased if the system has the capability to process more than the allocated size. These values are kept in one array, which need another command to retrieve the block of each image. The block in used will be kept in temp\_search and temp\_target for the maximum block size 30 x 30 each. If the retrievable position is incorrect, the final analysis will be incorrect as well. Many tests have been made to achieve this. One of the tests was to compare the input DN value with the dataset individual block by block and check the coordinate position.

Parts from that, the prototype have been created dynamically to accept different setting for different condition as discussed in the next section. All of the processes are encapsulated from the user. This includes all of the process such as creating data header and limiting windows search.

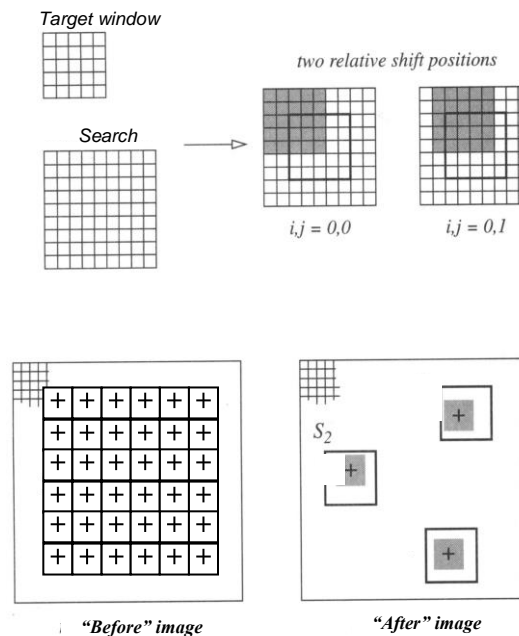


**Figure 2.** Area correlation for image cross correlation.

The most important process in the prototype is to keep the coordinate information efficiently and accurately. All of the DN values are kept in the search and target array as declared. The array size could be increased if the system has the capability to process more than the allocated size. These values are kept in one array, which need another command to retrieve the block of each image. The block in used will be kept in temp\_search and temp\_target for the maximum block size 30 x 30 each. If the retrievable position is incorrect, the final analysis will be incorrect as well. Many tests have been made to achieve this. One of the tests was to compare the input DN value with the dataset individual block by block and check the coordinate position.

Parts from that, the prototype have been created dynamically to accept different setting for different condition as discussed in the next section. All of the processes are encapsulated from the user. This includes all of the process such as creating data header and limiting windows search.

### 3. Automated imageodesy method (Basic Algorithm)

Basically, these method relies upon the fundamental statistical concept of a normal distribution as discussed on earlier Imageodesy typically compares thousands of pixels in the “before” image to another thousands of pixels in the “after” image in determining each displacement vector and may be capable of high accuracy at the high level of spatial precision by repeated local registration between various portions of the two images.

In order to calculate the cross correlation, an N by N “target” chip T (“Before” Image) sometimes called a “template” is selected in the reference image and M by M “search” chip S (“after” Image), with M greater than N, is selected in the distorted image or change image. The cross-correlation between the two areas is calculated by sliding the target chip over the central L by L region of search area as in the Figure 2, multiplying the two arrays pixel by pixel, and summing the result.

For example, 5 x 5 pixel target area (T) of “before” image and 9 x 9 search area of “after” image, (S), are shown at the top. Each block in the target window will be shifted and its DN arrays re-calculated to give its correlation coefficient (Equation 3) over the search and a possible shift location (L). After each shift over target, maximum cross-correlation coefficient will be marked which indicates the best fit on the search area. The only requirement for target and search areas is that the search area must be larger than the target window. Sub pixel precision can achieved by interpolating the L by L correlation surface to estimate the point of maximum correlation, which indicates the shift needed to register the two chips where L is equivalent 1 over the search area to give the normalized cross-correlation [31],[30],[22],[8].

By using equation 1, the cross-correlation prevents false correlation peaks arising from the changes in the image DN. Below is the source code (code 1) implemented using the equation above.

$$r_{ij} = \frac{\sum_{m=1}^N \sum_{n=1}^N (T_{mn} - \mu_T)(S_{i+m, j+n} - \mu_S)}{\sqrt{(\sum_{m=1}^N \sum_{n=1}^N (T_{mn} - \mu_T)^2) \sqrt{\sum_{m=1}^N \sum_{n=1}^N (S_{i+m, j+n} - \mu_S)^2}} \quad (1)$$

### 4. Displacement map

The core computation of the whole approach is the ground motion inference for a given image pixel. For example, for even relatively small images of 2050 x 2050 pixels, roughly four million vectors must be computed, raising the computational demands by four orders of magnitude above those required for a coarse-grained vector field. On machines

of the workstation class or current advanced computer, this calculation for ground motion vectors can be calculated in a matter of days.

A vector is calculated at each node on a grid by the use of (for example) 5 x 5 square of data from each image. The “before” and “after” image scenes are best fit matched to the nearest pixel, as determined by visual inspection (Manual GCP) . The before image is used still as the mapping base

and is held “constant”. For each vector determination,  $M \times M$  pixels of the before image are compared statistically for maximum correlation to a moving template of  $N \times N$  pixels in the after image.

Figure 3 is the schematic illustration of the use of sub pixel registration to infer displacement maps between image pairs. Shown are the “before” (A) and “after” (C) images and the displacement map generated by the Prototypes (B). The

This step generates a vector field of inferred ground motions from a pair of satellite images. This iterative procedure is terminated when sufficient accuracy is obtained. The resulting fault outlines can then be registered as important events. Below are the source codes to generate each vector point which represent matching point

```

static(m, l, mode);
Smn=0;
Tmn=0;
double sumProduct=0;
double co_variance=0;
for (int ctr=0; ctr<m*m; ctr++)
    {
        Tmn=(temp_target[ctr]);
        Smn=(temp_search[ctr]);
        sumProduct=sumProduct+((Smn-mean_b4)*(Tmn-mean_af));
    }
//for loop ctr
co_variance=sumProduct;
cross_coff[jum].cross_cof =((co_variance)/(sqrt(variance_b4*variance_a)));
cross_coff[jum].easting_af =point_col_af;
cross_coff[jum].northing_af =point_row_af;
    cross_coff[jum].easting_b4 = point_col_b4;
    cross_coff[jum].northing_b4 =point_row_b4;
    double te=cross_coff[jum].cross_cof;
    te=sqrt(pow(te,2));

point(, %lf, %lf, -1, -1, -1, 0). \n", (EQ.easting_b4+(2*b4cellsize)), (EQ.northing_b4+(2*b4cellsize))
    
```

**Code 1**

and for the shift

```

poly(2, [%lf, %lf, %lf, %lf], 1, 2, 0, 0, 0, 0, 255, 128, 128, 0). \n",
(EQ.easting_b4+(2*b4cellsize)), (EQ.northing_b4+(2*b4cellsize)),
(EQ.easting_af+(2*afcellsize)), (EQ.northing_af+(2*afcellsize))
    
```

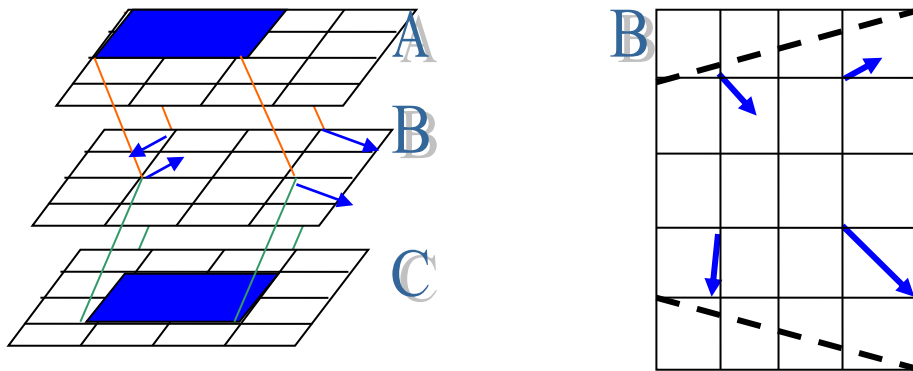


**Figure 3:** Inferring displacement maps between image pairs  
 (<http://mishkin.jpl.nasa.gov/spacemicro/intro.html>)

Each of the iterative will generate either point or line if the coefficient value is within the range. If the coefficient value is not in the range, vector generation will be ignored. Raw BIL dataset will be written, output to a file according to the user saved name and the ERMMapper vector Header will be created according the dataset automatically.

In principal, there are many type of corrections that must be accounted. For example, Sun- and view-angle differences can introduce spurious differences between scenes. In many remote-sensing applications, these effects are extremely important.

Radiometric differences are also possible as a result of vegetation and growth and other events. These are, in fact, often interesting processes in themselves, although they interfere with the specific task of measuring fault motion. For the datasets used here, they are not a major factor in any case. Yaw, pitch, and roll can also vary during a spacecraft over flight of a selected target, but again, this turns out to be a negligible effect for our problem.

### 5. Delta X and delta Y imagery

After a point has been matched every iteration using NCC, Delta X ( $\Delta x$ ) and Delta Y ( $\Delta y$ ) has been created to see the actual differences visually. Delta X ( $\Delta x$ ) and Delta Y ( $\Delta y$ ) are actually a values of possible shifted pixels cumulated in a dataset (\*.ers). Using these datasets histogram can be used to interpret the magnitude and the angle using below equation 4 and 5.

$$\Delta x = x_1 - x_2 \quad (4)$$

$$\Delta y = y_1 - y_2 \quad (5)$$

$$\alpha = \tan^{-1} (\Delta x / \Delta y) \quad (6)$$

Where subscript 1 is the DN from before “image” and subscript 2 is the DN from “after” image and the delta X is calculated using Equation 4 and Equation 5 is used for delta Y. Angle ( $\alpha$ ) of the shift can be calculated by using the equation 6. The process will generate similarly to Figure 4 Graph if no threshold have been set.

If the peak is pointed to 0 that means significantly, that both of images are match to exact coordinate. However the two peaks that are pointed to positive or negative show that the shift either the shift are move to left or right axis.

Practically, the histogram will look like in Figure 5. If the coefficient value is set to a range, the prototype may not generate shift. If this is the case, generated Histogram will not have the centroid peak. If the peak in the range of -1 are more compare to right peak then, this mean they are more movement going leftwards for Y axis or going downwards of X axis. This will be the opposite case if the peak is more on the right.

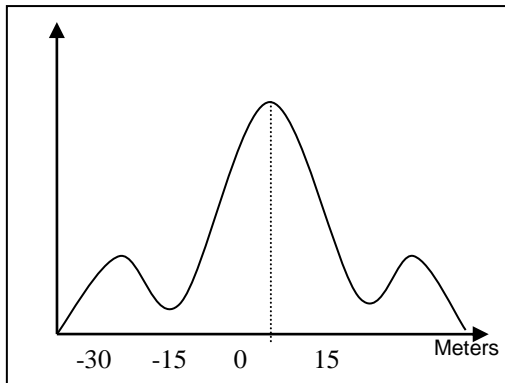


Figure 4: Histogram Delta X and Delta Y

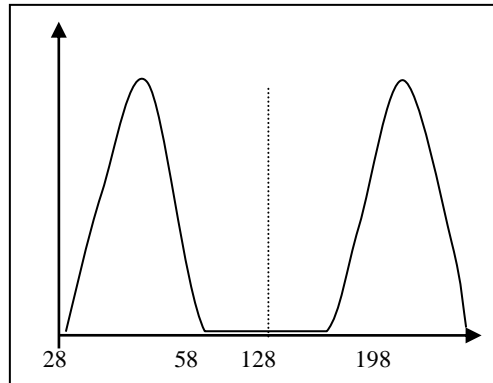


Figure 5: Coefficient Histogram

A part from Delta X ( $\Delta x$ ) and Delta Y ( $\Delta y$ ), a coefficient histogram is also needed. Literally, the coefficient values are between -1 and 1. For the purpose clear visual interpretation has been ranged between 28 to 228. Threshold value which the user has specified will make the range in the histogram above the threshold value as shown in the Figure 5. If the threshold value is set at 0.70, then histogram curves will start at 58 or 198.

### 6. Result Founding's

While the program calculate the coefficient and match the pixels in both of the image, all this information are also being stored in the database in Microsoft SQL Server with a different dates or coefficients variable. Examples of data are shown as in Table 1. The current database design is follows. The follow database will analyst using Unsupervised K-Mean Clustering.

Figure 6 Database Design in SQL Server

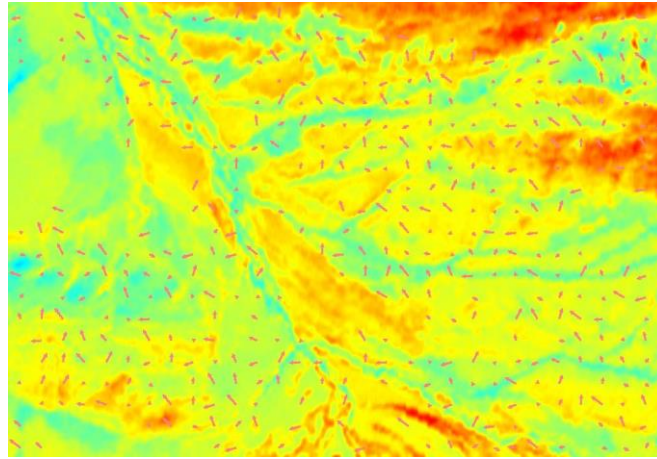
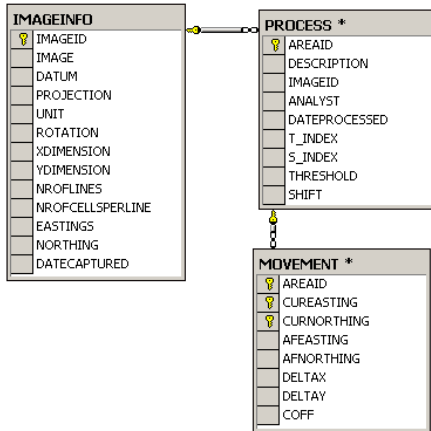


Figure 7: Displacement Map and the overlay over dataset using pseudocolor Examples result for Image Change Detections using Imageodesy.

Table 1 Data comparison after NCC using Excel to Generate

Eastings Before	Northing Before	Eastings After	Northing After	Value Coefficient	Changes Easting	Change Northing
297639.006	4042277.203	297594.006	4042322.203	-0.97526	-45	45
297774.006	4042277.203	297819.006	4042337.203	-0.927716	45	60
298044.006	4042277.203	298044.006	4042322.203	-0.96821	0	45
298179.006	4042277.203	298209.006	4042322.203	-0.964162	30	45
298584.006	4042277.203	298599.006	4042322.203	-0.879086	15	45
298719.006	4042277.203	298674.006	4042277.203	-0.997689	-45	0
298989.006	4042277.203	299004.006	4042262.203	-0.960686	15	-15
299124.006	4042277.203	299109.006	4042292.203	-0.910279	-15	15
299934.006	4042277.203	299904.006	4042337.203	-0.803248	-30	60

The pattern found from this figure 7 has shown that this location has many activities and movements based on the Normalize Calculations. Another area was also tested for detecting the pattern movement. A threshold was set in order to select or search for highest correlation coefficient value that has been specified by the user. Currently a default value of 0.7 has been set. Because the dataset has different sun-illumination and different seasons, the variance are too huge in different. Clearly this difference can be observed in Figure 8. This might cause the coefficient value being out of range. Another threshold has been inserted in the program to remove this problem. By putting this threshold, those points will be ignored. These features are shown in Figure 8. The empty areas in the image represent ignored points which mean the area has low correlation or out range.

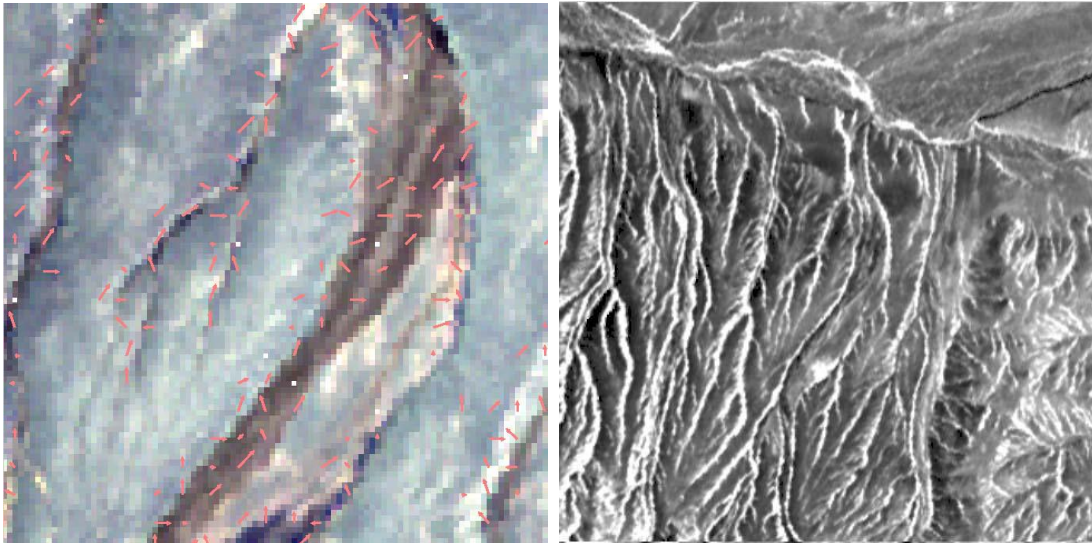


Figure 8: A generated vector of the displacement (shift) overlay to the RGB Kunlun before Earthquake.

After the process, the prototype will generate delta X, delta Y and coefficient histogram with vector displacements for the next analysis. The processes were performed twice with rectified and unrectified of the “before” and “after” image at the same area. The vectors are represented by the arrow in red (Figure 8 ) which showed the point shift from the “before” coordinate to “after” coordinate.

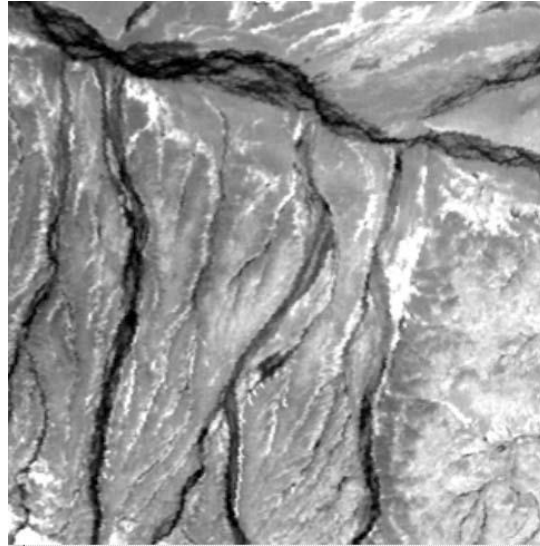


Figure 9: Area D: - sample of an area from the North-West Mountain in Kunlun. (Left- Before Earthquake and Right-After Earthquake)

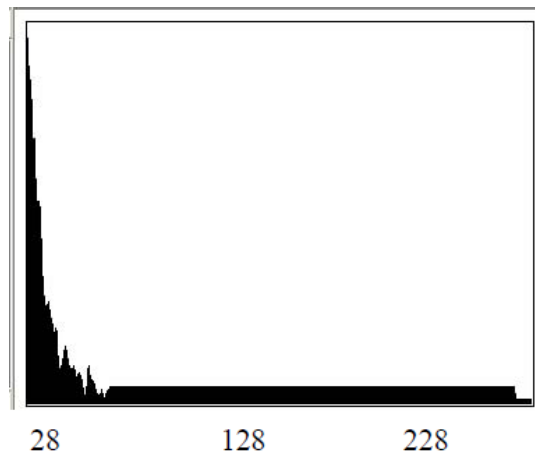


Figure 10: Histogram of Coefficient

The coefficient values which have been calculated will be used to get the matching point and a table is created. This table is a sample of the selected coefficient value with the highest matching after the process of using “before” and “after” image. Histogram (Figure 10) has been generated to show the range used.

Figure 11 has 2 histogram of delta X cover the same area using a rectified and unrectified image. Obviously, the shift (around -45m) on the left of the unrectified image has significantly dropped after the rectification. Here, the histogram showed shifts to be more to right in the X axis.

Delta Y (Figure 12) showed a different direction. The shift are more toward the downwards of Y axis. The average of the shift angle is around -45 degree to -53 degree to the south east.

The angles are calculated by taking the lowest and the highest shifts corresponding to those shifts discussed in Figure 14 and Figure 15 using equation 6.

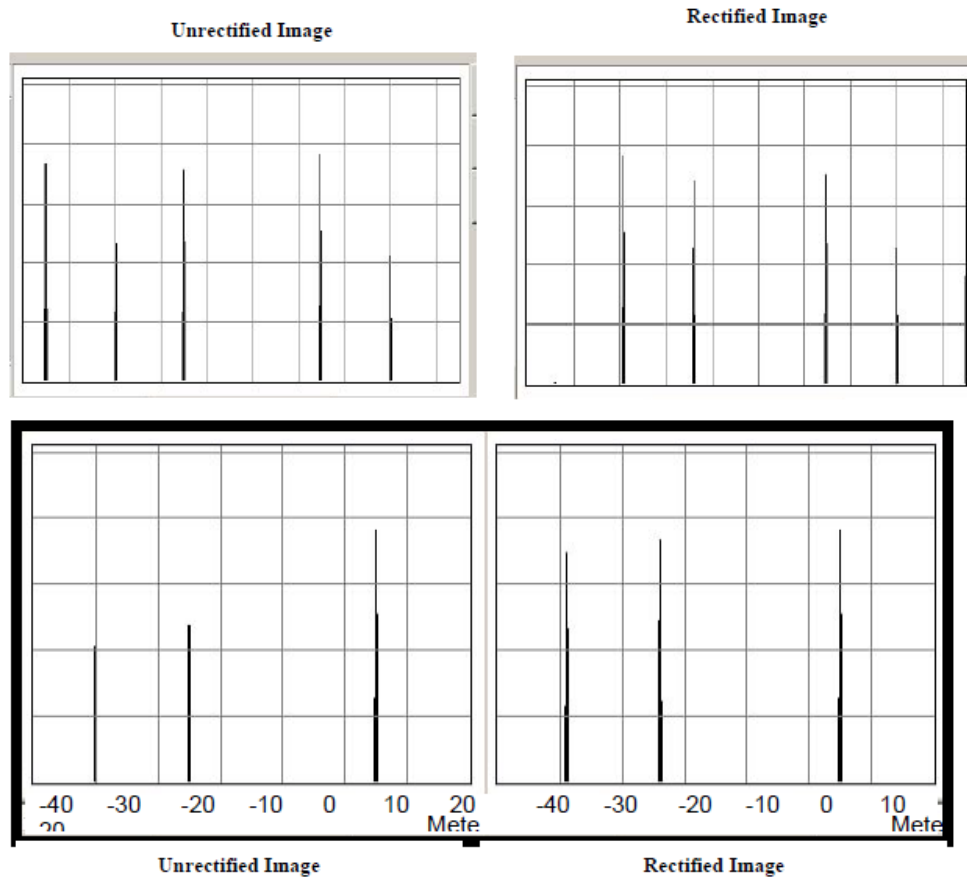


Figure 11: Histogram of Delta X in meter using Non-Cumulative Style

Figure 12: Histogram of Delta Y in meter using Non-Cumulative Style

### 3. Computational cost

NCC in computation time has to mask pixels and multiplied them. The sum of product operation has the main effect for computational cost and then lengthens the process in the dataset imagery. Below, Table 2 shows the comparison time for Normalized Cross-correlation using different M and N.

Table 2: Comparing Computational Cost – Ncc (µS/ Pixel)

M	N	SPEED
5	9	0.10
9	15	0.27
15	30	0.35

The size of an image with 2050 x 2050 pixels will have 4202500 pixels to be calculated. In order to get a medium accuracy with the result block by block precision, M as shown is equal to 9, N is equal to 15 and L is equal to 9,

Therefore,

Computational Cost

$$= [(4202500 / (M * M)) * SPEED] / (60 \text{ SEC} * 60 \text{ MIN} * 25 \text{ HOUR})$$

$$= 1.56 \text{ days}$$

Based on AMD Duron 1 GHz and with 384 MB ram.

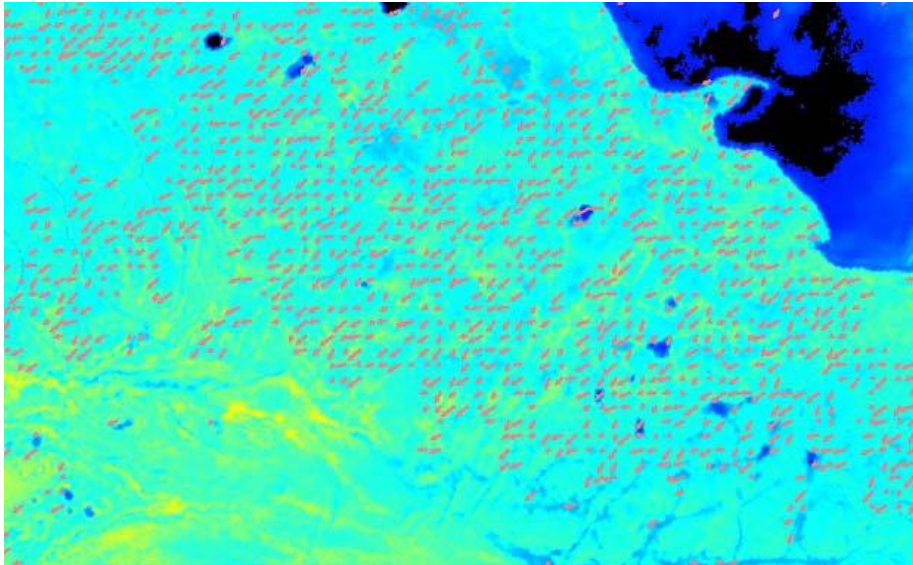


Figure 13:- Displacement of the area A and the overlay of unrectified dataset.

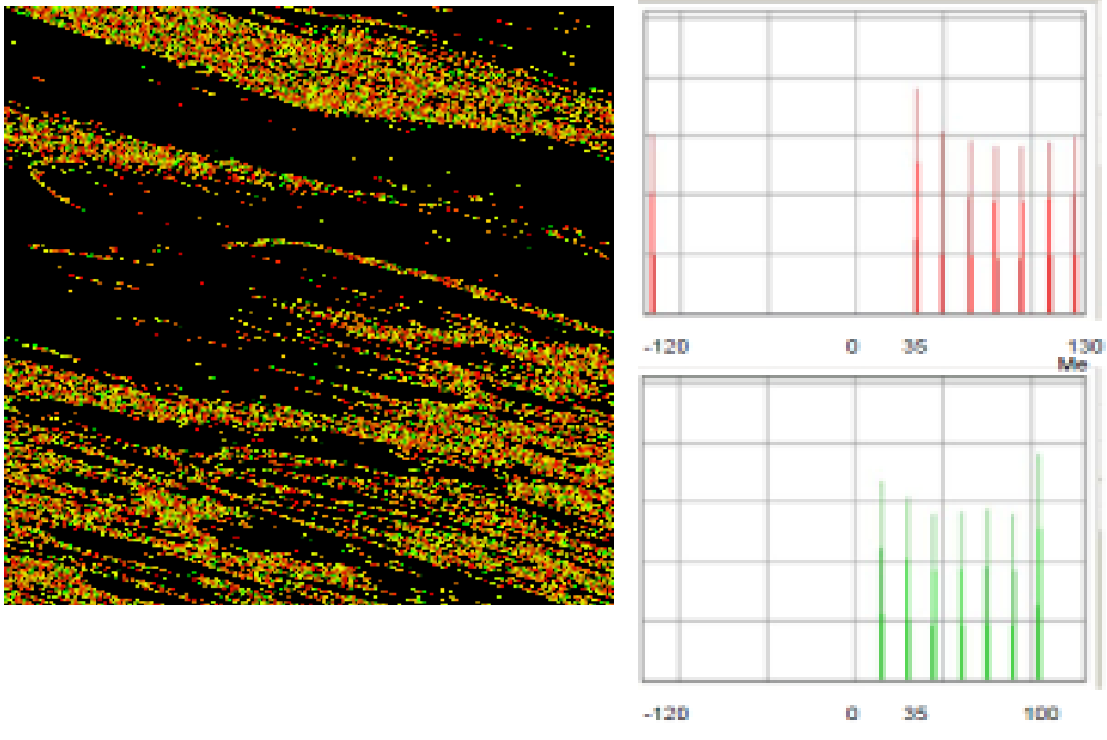


Figure 14:- Delta Y in Green and Delta X in Red representing false colour composite and for colour in histograms for unrectified

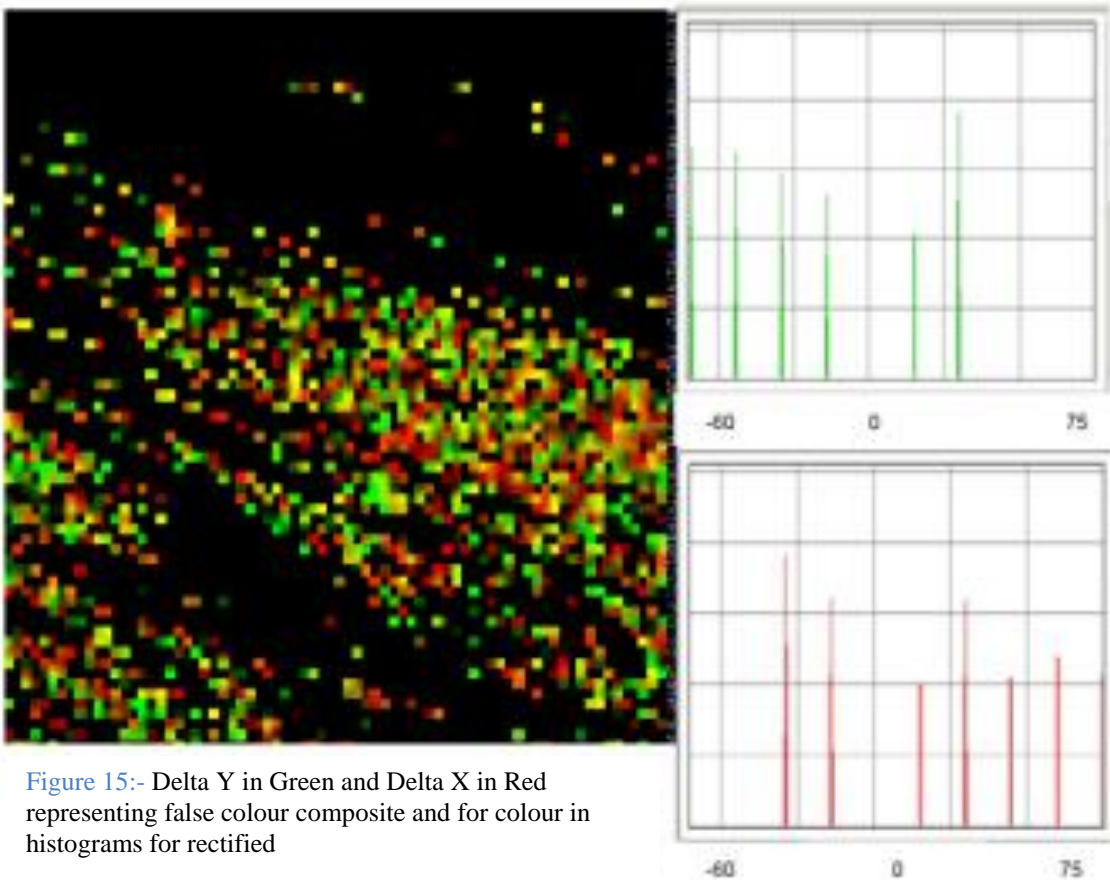


Figure 15:- Delta Y in Green and Delta X in Red representing false colour composite and for colour in histograms for rectified

In order to obtain high precision and accuracy on pixel by pixel basis, the prototype will need up to 8 days of processing time based on 2050 x 2050 pixels. Due to the limited time, next section, will discuss the result based on the medium accuracy with result block by block.

The areas cover at between 283420E and 4042385N to 314094 E and 4011553 N, near the lake and the epicentre of Kunlun China. The process took 30 hours (on a machine using 1 GHz speed CPU with a memory of 384 MB) each on unrectified and rectified dataset of “before” and after the Earthquake using  $M = 9$  and  $N = 15$  and  $L = 9$ .

The areas cover at between 281098E and 4027517N to 291606 E and 4018226 N, near the alluvial fan south of the lake. There are lots of shiftings and changes in the alluvial fan itself as shown in Figure 15a.

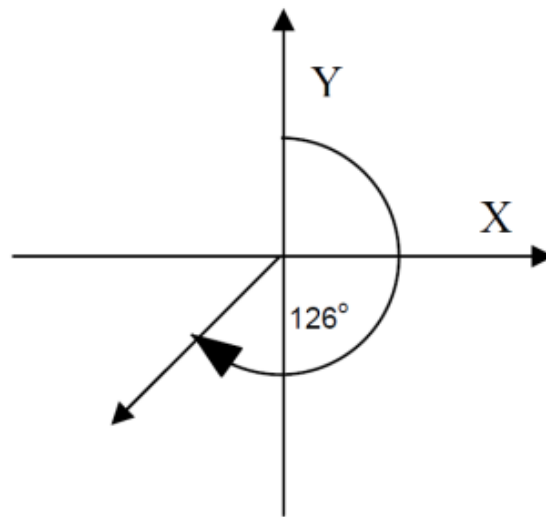


Figure 15a:- Shifting's and Changes in alluvial fan

By estimating the delta X and delta Y using the histogram as shown in Figure 6.11, the maximum possible shifts were -30 and 30 respectively. Therefore the possible shift angle is  $315^\circ$  with 42.42m ( $\approx 2.8$  pixel) magnitude. These shiftings can be seen in Figure 16.

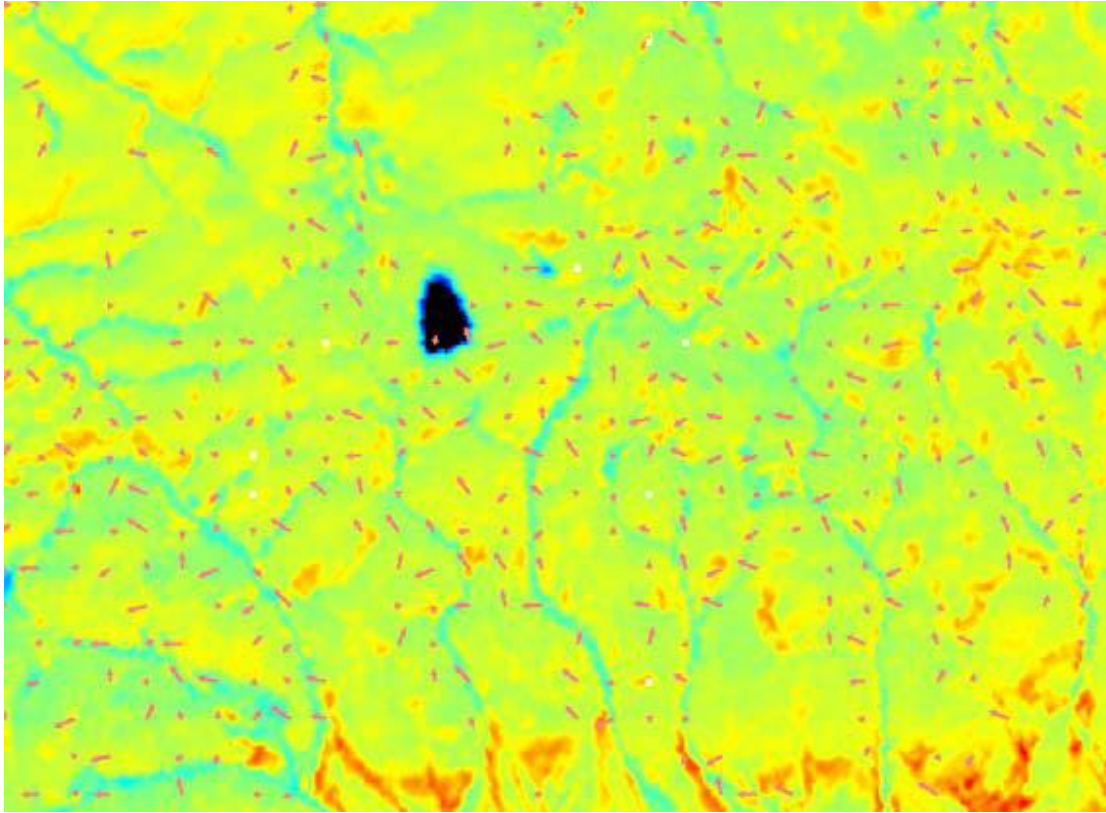


Figure 16:- Displacement of the area B and the overlay dataset using pseudocolor.

Based on the observation that the trend pattern that has been created. This prototype could be used to calculate the average angle and the magnitude automatically and then draw average pattern trend for each specific size windows to show a greater accuracy of trend pattern (Figure 17). Because of some the areas have moved in many directions and angles, the actual displacements could not be represented very accurately.

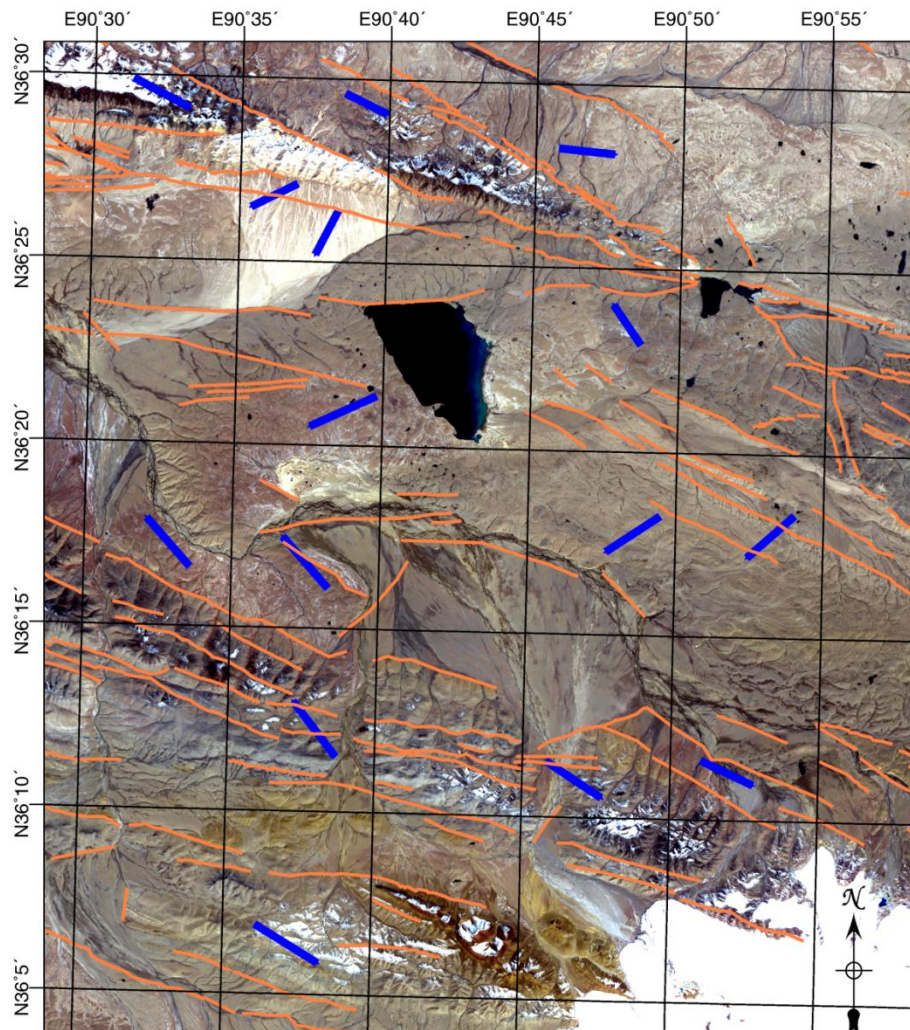


Figure 17: Displacement Pattern

### 3. Fault directions

NCC is very sensitive to shape and edges and because of its feature, faults are easily distinguished. One obvious process of great physical interest is the motion of surface faults during the course of the earthquake. This detection can be clearly seen from Figure 18.

Observed analysis (blue vector) made were quite rigid and straight compares to the generated vector displacements which follows the pixel by pixel changes. Significantly the detections were much accurate. However, the final results still need the geologist to interpret or ground truths for better understand of the features changes.

Normalized Cross Correlation (NCC) has been used widely because it can cope with noisy images and uniform change in brightness. But when the scene involves partial occlusion of objects or saturation (highlight), this sum of multiplication-based correlation techniques sometimes fails to capture true position, while it is good to measure some slight change in brightness [22]. For the effectiveness use of measuring Sub Pixel level of earthquakes, sun-angle and view angle differences between imagery must be avoided. Shadows will not match between scenes due to different sun

positions. Likewise, radial distortion of topographic features in images will differ between images different view angle. The other major source of geometric noise, results arises from the sensor attitude and altitude differences. These techniques provide useful tools for measuring Earthquake. As for now, the detectable shift or movement is 15 m or equivalent to 1 pixel. The vectors provide statistically significant result that can be modeled to remove geometric noise and thereby obtain precise displacement directions over a wide area. Fault breaks in remote location might be located by the vector.

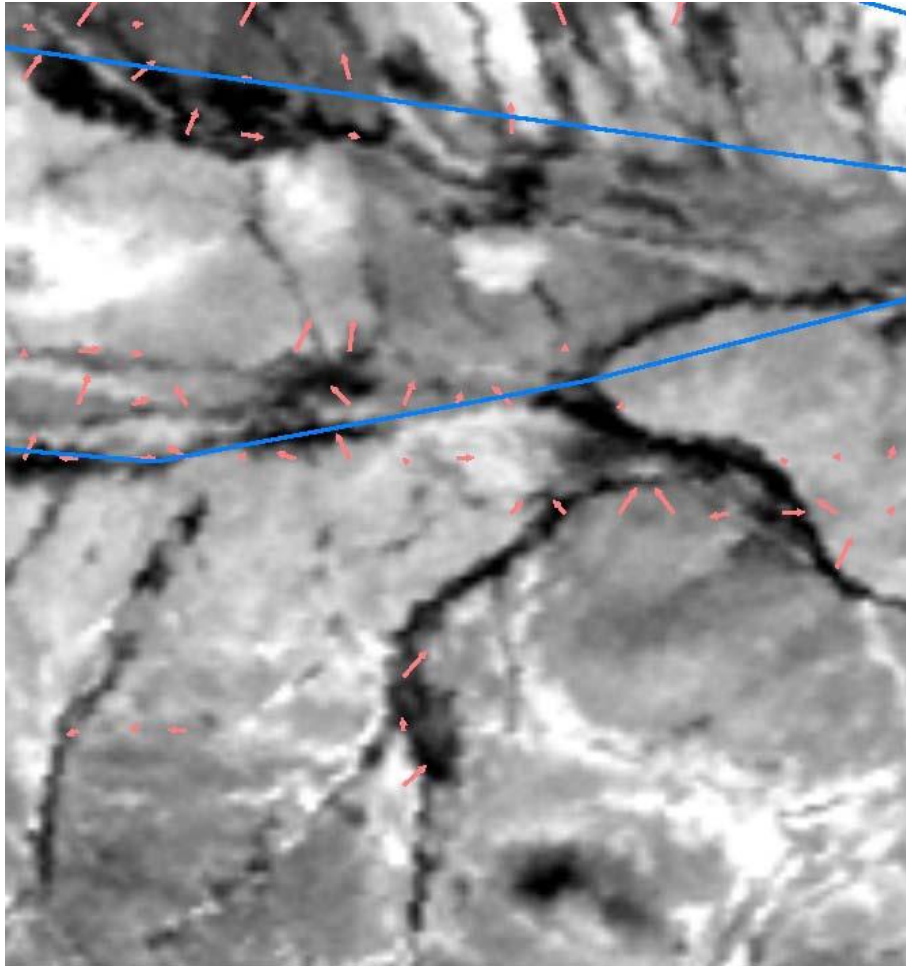


Figure 18:-Fault Detection (In Blue is the observed fault drawn and red arrow is the vector to show fault lines.)

From the analysis, most displacements in the area are within 1 pixel. However, due to the mismatch of the “before” and “after” Imagery, the final results therefore are spatially biased correlated pattern. The measured displacement may not be necessarily the displacement itself, whereby it could be also the geometric distortion or mismatch points. The images supposed to be rectified from the beginning in order for an accurate matching to be achieved. Unfortunately, images are degraded due to resampling. This problem could be solved using image differencing and removed by the correlation procedures by image masking [5]. In areas where radiometric change is pervasive such as agricultural fields,

subresolution matching of edges in the image can form boundaries which may be possible as an alternative procedure. But this procedure could not be implemented yet due to time constraint. Overall performance, the method used in this project is considered to be successful in measuring the angle of the displacement. This displacement however needs ground truth in order to access and understand the change and the movement. A part from that, the prototype could also be improved to extract more accurate information automatically. Since in this project, final stages of pattern trends were still done manually and the prototype could also use the pixel (DN) resampling to increase the precision.

## Acknowledgment

I would like to express my gratitude to my Supervisors, Dr. Shafry (Universiti Teknologi Malaysia), Dr J.G. Liu and Dr. Philippa Mason of Earth and Resource Department at Imperial College London, for the extensive advice throughout the progress of this study.

## References

- [1] Bolshakova, N, 2001, An integrated tool for microarray data clustering cluster validity assessment.
- [2] Bolshakova, N, 2001, Cluster validation techniques for genome expression data
- [3] Bolshakova, N, 2001, Improving Expression Data Mining Through Cluster Validation
- [4] Crippen, R. E., 1992, Measurement of sub resolution terrain displacements using SPOT panchromatic imagery. : International Journal of Remote Sensing Vol 15, no. 1 page 56-61.
- [5] Crippen R.E. and Blom, R.G.,1992. Mapping of the Horizontal Strain Field of the 1992 Landers Earthquake by Imageodesy, EOS Transactions of the American Geophysical Union, 73(43):374.
- [6] Crippen, R. E., 1992. Measurement of subresolution terrain displacements using SPOT panchromatic imagery. EOS Transactions of the American Geophysical 15(1): 56-61.
- [7] Crippen, R. E. and Blom, R. G.,1996. Detection, measurement, visualization, and analysis of seismic crustal deformation. In: Proc. 11th International Thematic Conference on Geologic Remote Sensing, (ERIM, Ann Arbor, Michigan). 1: I-298.
- [8] Dani P. and Chaudhuri S., 1995. Automated Assembling of Images: Image Montage Preparation, Pattern Recognition 25(3):431-445.
- [9] David. K., 1998. Programming Microsoft Visual C++. Fifth Edition, Microsoft Press. 1153 pages.
- [10] David. W., 2000. Mathematic: Simple tool for geologist. Second Edition. Chapman and Hall, Inc. 201 pages
- [11] Dury S.A. .1993. Image Interpretation in Geology 2nd. Chapman and Hall, London. 290 pages
- [12] ER Mapper 6.0, 2000. Software Development Kit, Earth Resource Mapping Pty Ltd. Everitt B., Cluster Analysis, London: Edward Arnold, 1993
- [13] F. Azuaje, 2002 "A cluster validity framework for genome expression data", Bioinformatics, Vol. 18, 2002, pp. 319-320
- [14] Lillesand, T.M. and Kiefer, R.W. (2000). "Remote Sensing And Image Interpretation", John Wiley & Sons, New York
- [15] Liu Juan Guo 2000. Smoothing Filter Band Based Intensity Modulation: a Spectral Preserve Image Fusion Technique for improving Spatial Details. IJRS, 21, No 18, 3461-3472
- [16] Liu Juan Guo 2000 and Moore J. McM, 1998. Pixel Block Intensity Modulation: adding Spatial Details to TM Band 6 Thermal Imagery IJRS, 21, No 18, 3461-3472
- [17] Liu Juan Guo , Moustafa Ghanem, Vasa Curcin, Christian Haselwimmer, Yike Guo, Gareth Morgan, Kyran Mish 2006
- [18] Distributed, high-performance earthquake deformation analysis and modelling facilitated by Discovery Net
- [19] Halkidi.M, Batistakis.Y, Vazirgiannis. M.,(2001), On Clustering Validation Techniques
- [20] Khamarrul A.R (2003) An Appropriate GPS Technology for Landslide Monitoring at East-West Highway, Perak, Malaysia
- [21] S.A Dury (1993). Image Interpretation in Geology (2nd). Chapman and Hall, London.

- [22] Lewis J. P. ,1995. Fast Template Matching, Vision Interface, p. 120-123,.
- [23] Lillesand, T.M. and Kiefer, R.W., 2000. "Remote Sensing And Image Interpretation", Fourth Edition John Wiley & Sons, New York. 724 pages.
- [24] Liu J.G., 2000. Smoothing Filter Band Based Intensity Modulation: a Spectral Preserve Image Fusion Technique for improving Spatial Details. IJRS, 21, No 18, 3461-3472
- [25] Jensen, J.R., 1986. Introductory Digital Image Processing –A Remote Sensing Perspective, Prentice Hall, Englewood Cliffs, NJ, pages 102-105
- [26] Hanssen R. F. , 2001. Radar Interferometry:- Data Interpretation and error analysis, Optima Grafische Communicatte. 308 pages
- [27] Herbert S. ,1987. Artificial Intelligence: Using C. McGraw-Hill. Inc. 411 pages.
- [28] Kaneko S and Satoh Y.I.S., 2002. Using selective correlation coefficient for robust image registration, Pattern Recognition, Pergamon p 1-9, 2002
- [29] Tierney K., 1998. Improving Earthquake Loss Estimation: Review, Assessment and Extension of Loss Estimation Methodologies, Uni. of Delaware. pages 1-14
- [30] Richards, J. A ,1995. Remote Sensing Digital Image Analysis, Springer-Verlag, Berlin, pages. 54-57.
- [31] Schowengerdt R.A, 1997. Remote Sensing Model and Methods for Image Processing, Second Edition. Academic Press 522 pages.
- [32] Tsuneji S.R.R and Yukoo H., 1987. Applied Mathematic for Earth Scientist, Terra Scientific Pub Co. Tokyo. 435 pages.
- [33] Tom A., 1992. Earthquake Prediction: Science on Shaky Ground? The Scientist 6[14]:15.
- [34] Wan Aziz W.A , (2003) An appropriate GPS technology for landslide monitoring at east-west highway, Perak, Malaysia
- [35] Dr. Dan Russell, 1999, <http://www.kettering.edu/~drussell/demos.html>) ( Laste seen on the 14 February 2006)
- [36] Paul S., Dean C, Crippen R. and Blom R. 1999, <http://www.cacr.caltech.edu/Publication/annreps/annrep95/earth1.htm> Photographing Earthquakes from Space on Earth Sciences (Last seen on the 15 July 2002)
- [37] Paul S., Dean C, Crippen R. and Blom R. 1999, [http://mishkin.jpl.nasa.gov/spacemicro/SCALABLE\\_PAPER](http://mishkin.jpl.nasa.gov/spacemicro/SCALABLE_PAPER) Scalable Scientific Data mining on Massively Parallel Computer (Last seen on 2 June 2002)
- [38] QUAKEFINDER: Photographing Earthquakes from Space (Last seen on 2 June 2002) <http://www-aig.jpl.nasa.gov/public/mls/quakefinder/>
- [39] Garson <http://www2.chass.ncsu.edu/garson/pa765/garson.htm>(Last seen on the 30 July 2002)
- [40] Ebmj <http://bmj.com/collections/statsbk/index.shtml> (Last seen on the 14 Aug 2002)
- [41] USGS National Earthquake Information Centre <http://mapping.usgs.gov/> (Last seen on the 4 Jan 2006)
- [42] [http://mishkin.jpl.nasa.gov/spacemicro/SCALABLE\\_PAPER](http://mishkin.jpl.nasa.gov/spacemicro/SCALABLE_PAPER) Scalable Scientific Datamining on Massively Parallel Computer
- [43] <http://www-aig.jpl.nasa.gov/public/mls/quakefinder/> QUAKEFINDER: Photographing Earthquakes from Space.